JOURNAL OF CATALYSIS 50, 319–329 (1977)

Temperature-Programmed Desorption of N_2, Ar, and CO_2 Encapsulated in 3A Zeolite

YUN-CHEUNG CHAN* AND ROBERT B. ANDERSON

Department of Chemical Engineering and Institute for Materials Research, McMaster University, Hamilton, Ontario, Canada L8S 4L7

Received May 23, 1977

Temperature-programmed-desorption (TPD) studies with a linear heating rate and He as a carrier gas were made on N_2, Ar, and CO_2 encapsulated in 3A zeolite. N_2 and Ar desorb only slowly at room temperature, and CO_2, more rapidly. In TPD experiments, N_2 and CO_2 gave one peak, 290–340 and 194–240°C, respectively, depending on the heating rate. Argon had one peak at 340–360°C and a second incompletely resolved peak at temperatures above 500°C. Possibly the second peak for Ar results from desorption from β cages. Using Fick's law equations for this unsteady-state nonisothermal diffusion process and taking into account the particle size distribution, the TPD data for several heating rates could be predicted with reasonable accuracy using two adjustable parameters. One of these, the activation energy for diffusion, had values of 17.3, 13.0, and 15.8 kcal/mol for N_2, CO_2, and Ar, respectively.

INTRODUCTION

The rate of sorption processes in zeolitic molecular sieves are often controlled by activated diffusion, particularly when the size of the adsorbate is about the same as that of the apertures of the zeolite. For activated diffusion, the diffusivity, D, may be expressed as $D = D_0 \exp(-E/RT)$. If the activation energy, E, is large, adsorption and desorption may not occur at some low temperature, but may proceed at substantial rates at higher temperatures. At the higher temperature, however, the amount of gas held by the zeolite at equilibrium may be small unless high pressures are used.

Breck (*1*) heated a 3A zeolite at 350°C in CH_4, Ar, and Kr at high pressures and cooled the sample to room temperature before depressurizing the system. Substantial quantities of gas were more or less permanently held in the zeolite at room temperature; Breck called this process "encapsulation." When the zeolite was heated, the gas was evolved. These gases do not adsorb in appreciable amounts on the 3A zeolite at room temperature and atmospheric pressure. At 350°C and high pressures, the amount of encapsulated gas approached the adsorption capacity of A zeolites; for example, 105 and 109 cc (STP)/g for CH_4 and Ar, respectively, at 2650 atm. On storage at room temperature, about 93% of the CH_4 remained after 37 days and 71% of the argon after 79 days.

Walker and co-workers (*2*, *3*) measured the rate of desorption of gases from 3A zeolite on decreasing the pressure from 1.4 to 1 atm at 300–400°C, using a sensitive volumetric apparatus. Activation energies of 14 and 16 kcal/mol were obtained for Ar and N_2.

* From the Master of Engineering thesis of Y-C. Chan, McMaster University, October 1976. Present address: 111-58 Ave., S. W., Calgary, Alberta, Canada.

ISSN 0021-9517

Barrer and Vaughan *4–6* encapsulated rare gases in a variety of low-porosity zeolitic material, including tridymite, cristobalite, sodalite, and cancrinate, at high pressure and temperature and measured initial desorption rates. Of particular interest to the present work, activation energies for desorption from sodalite were 30 and 52 kcal/mol for Ar and Kr, respectively.

The present paper describes temperature-programmed desorption (TPD) of N_2, Ar, and CO_2 encapsulated in a commercial 3A zeolite using a linear increase of temperature. By applying solutions of Fick's law for cubes appropriately to the nonisothermal unsteady-state diffusion process and taking into account the distribution of particle sizes, the entire desorption curves for several heating rates can be fitted with reasonable accuracy using only two parameters. TPD has been described by Cvetanovic and Amenomiya (*7*), Smutzek, *et al.* (*8*), and Dawson and Walker (*9*).

The structure of A zeolite is well known (*10*); it contains large cavities (α cages) with diameters of 11.4-Å that are interconnected by six apertures with diameters of 4.2 Å and smaller cavities (β or sodalite cages) 6.6 Å in diameter connected to the α cages by apertures 2.2 Å in diameter. Sodium and potassium ions partly block the apertures so that molecules larger than H_2O and NH_3 are not adsorbed at room temperature on the K^+-exchanged A zeolite or on the commercial 3A which is a 50% K^+-exchanged NaA zeolite.

EXPERIMENTAL

A sample of 3A molecular sieve powder was kindly supplied by the Linde Division of Union Carbide. Analysis by atomic absorption gave the atomic ratio of Na to K as 1.02. Hence, the sample was a 50% potassium-exchanged NaA. All samples were initially evacuated to pressures less than 10^{-5} Torr at 450°C for 15 h, and the weight loss in this treatment was 17–19%. Desorption data are reported per gram of dry sample.

Encapsulation of N_2, CO_2, and Ar was accomplished by heating the evacuated sample at the highest pressure attainable from gas cylinders in an autoclave at 350°C, followed by cooling to room temperature before depressurizing the system. The evacuated samples in glass tubes with male ground joints were transferred to the autoclave, and the head was attached, all with a stream of adsorbate flowing through the system. The autoclave was evacuated with a rotary oil pump and then was pressurized to about 135 atm (54 atm for CO_2). The valve to the autoclave was closed, and the unit was heated rapidly to 350°C and was held at this temperature for 8 h. Finally, the autoclave was cooled slowly to room temperature over a period of 12 h before depressurizing. With the adsorbate flowing through the autoclave the head was removed, and the sample tubes were closed with a greased ground glass cap. Samples were transferred to the tubes for temperature-programmed desorption (TPD) or volumetric measurements in a dry box with dry nitrogen maintained at a pressure above atmospheric pressure. In the transfer steps, contamination of the sample by atmospheric moisture was prevented. The sample in the adsorption or TPD tubes was evacuated at room temperature for 30 min before use.

Temperature-programmed desorption (TPD) was performed in a dynamic system using helium as a carrier gas and a linear heating rate. The sample was heated in a tubular electrical furnace constructed with the heating wire placed near the inner surface of the refractory to minimize temperature lags. The furnace temperature was increased linearly by driving at a constant rate the potentiometer knob of a proportional controller connected to a chromel–alumel thermocouple positioned between the furnace and sample tube at the position of the sample. Temperatures within the

sample were measured by a thermocouple positioned within a glass tube at the center of the sample by reading a digital voltmeter at frequent intervals.

The knurled potentiometer knob of the controller was driven by a rubber wheel connected to a synchronous motor. By changing the diameter of the rubber wheel or changing to another motor the heating rate could be varied over a wide range; 3–17°C/min was used in the present work.

A flow diagram of the flow system is shown in Fig. 1. Helium from the cylinder and regulator passed through a needle valve, a capillary flowmeter, a cold trap, the reference side of a thermal conductivity cell (TCC), the sample tube, a second cold trap, the detection side of the TCC, and finally to a soap-film flowmeter. The two cold traps, dry ice–acetone, removed water, if present, in the gas streams. A water vapor-saturation tube was included in the system so that water vapor at about 24 Torr could be introduced if desired. A gas chromatograph injection valve with several loops of known volume was also included for calibrating the response of the recorder. The thermal conductivity cell was Gow-Mac Model 10-952 with tungsten filaments, and the TCC response was recorded by a recording potentiometer with a ball-and-disk integrator.

The capillary flowmeter permitted continuous measurement of carrier gas flow. With fine powders the pressure drop in the bed is sufficient that the helium flow decreases about 4%, from 25 to 500°C, due to increasing gas viscosity, resulting in about a 5% increase in sensitivity but no change in the baseline. The lower portion of the U-shaped desorption tube was made of silica, which was attached to the upper Pyrex part by graded seals. The sample rested on a silica sintered disk, the carrier gas flowing upward through the disk and sample. The helium flow was 40 ml/min. The time lag from the desorption tube to detector was 22 s; this factor was included in the analysis of the data.

The total amount of gas released from the zeolite was also determined in a volumetric adsorption apparatus; however, these data were obtained only to check the values from the TPD experiments. The total volumes desorbed by the two methods generally agreed well as shown by the data in Fig. 2, where the amount desorbed is plotted against the square root of time of storage of the encapsulated sieve. This figure also shows that Ar and N_2 desorb or

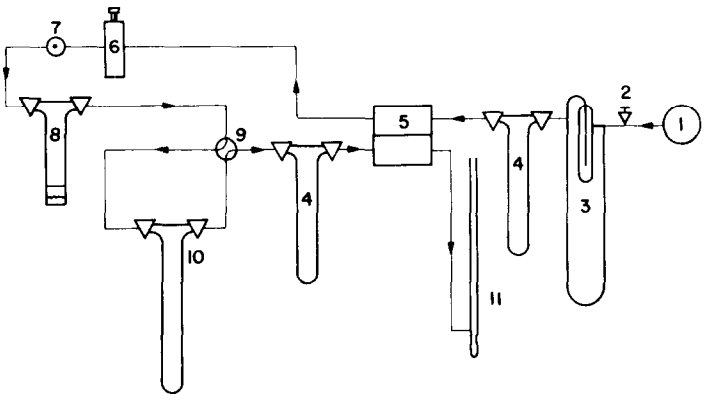

FIG. 1. Schematic diagram of the TPD system: (1) He from a cylinder, (2) needle valve, (3) capillary-flowmeter, (4) cold traps, (5) thermal conductivity cell, (6) plunger-type injection valve, (7) septum injection port, (8) water saturator, (9) four-way stopcock, (10) sample tube, and (11) soap-film flowmeter.

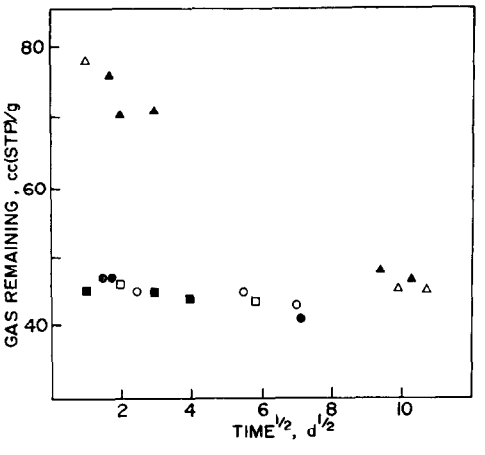

FIG. 2. Loss of encapsulated gas at room temperature; circles are N_2, triangles, CO_2, and squares, Ar. Open symbols denote volumetric data; solid symbols, TPD.

"leak" only very slowly at room temperature, and CO_2 does so relatively rapidly.

Particle size distributions were determined with a Phillips transmission electron microscope at magnifications of 4500–13,000. Adequate dispersion of the powder was obtained by stirring 2 g of zeolite in 100 ml of methanol for 1 h. A drop of standard latex material with diameters of 0.234 μm $\pm$ 4% was added to the suspension. The suspension was sprayed on Formvar films supported on copper grids. The specimens were coated with a layer of evaporated carbon before use. About 400 particles were measured; they were cubes, but the larger particles had their edges truncated at 45° to the cubic faces.

After desorption to 400 and 700°C, the fresh zeolite and samples were examined by powder X-ray diffraction using a Debye–Scherrer camera with copper $K\alpha$ radiation. The samples were hydrated and placed in glass capillaries 0.1 mm in diameter and were exposed for 4 h. The patterns reported in Table 1 show that the lattice parameter (12.3 Å) was the same for all samples; however, some of the reflections became weaker for the heated samples, particularly for those heated to 700°C. To examine the possibility that lattice distortions can be produced by or accompany desorption, the adsorption of N_2 at −78°C was measured

TABLE 1

X-Ray Diffraction Patterns of Hydrated Samples of 3A Zeolite

Fresh sample			Sample desorbed at 400°C			Sample desorbed at 700°C		
θ	d, Å	I^a	θ	d, Å	I^a	θ	d, Å	I^a
7.2	12.30	S	7.2	12.30	S	7.2	12.30	S
10.2	8.71	S	10.0	8.87	S	10.0	8.88	S
12.5	7.12	M	11.2	7.94	M	12.4	7.18	W
16.2	5.53	M	15.9	5.63	W	15.9	5.63	VW
17.5	5.13	VW	—	—	—	—	—	—
20.4	4.42	VW	—	—	—	—	—	—
21.7	4.17	S	21.6	4.19	M	21.6	4.19	M
22.8	3.98	W	—	—	—	22.9	3.96	W
24.0	3.79	S	23.9	3.81	S	23.8	3.82	S
25.0	3.65	VW	—	—	—	—	—	—
26.0	3.52	M	26.0	3.52	W	26.0	3.52	W
27.2	3.37	S	27.1	3.38	M	27.1	3.38	M
29.0	3.18	W	29.1	3.17	W	—	—	—
29.9	3.09	S	29.9	3.09	S	29.8	3.10	S
30.9	3.00	M	30.7	3.02	W	—	—	—
32.6	2.86	M	32.4	2.88	M	32.5	2.87	W

[a] Intensity: S, strong; M, medium; W, weak; VW, very weak.

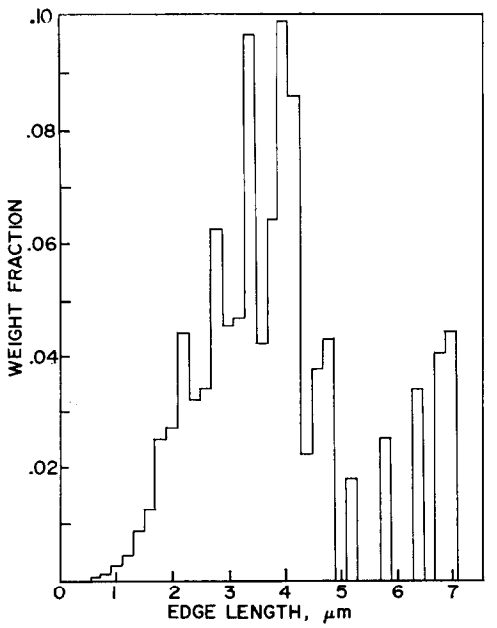

FIG. 3. Particle size distribution for the 3A zeolite.

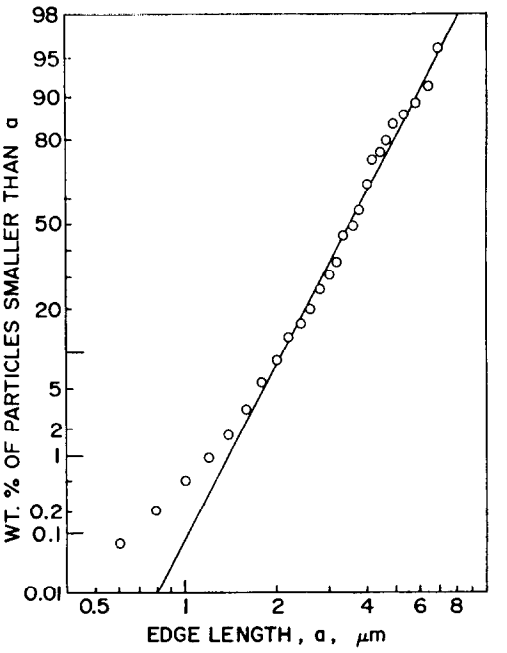

FIG. 4. Log-normal particle size distribution plot.

on sieves heated to 400°C. The maximum adsorption was 3 ml of STP/g, compared with 60 for a 4A zeolite. Hence, the pore openings were not permanently enlarged in the thermal desorption.

EXPERIMENTAL RESULTS

The particle size distribution, edge length of the cubes, on the basis of weight is given in Fig. 3. The log-normal distribution fits these data reasonably well for particles larger than 1 μm, about 98% of the weight, as shown in Fig. 4. The normal distribution fits only the middle 75% of the weight of the sample. For this reason and because the normal distribution may permit negative particle sizes in some calculations, the

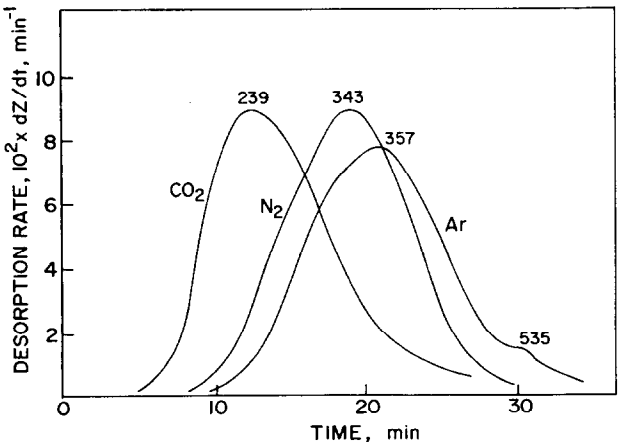

FIG. 5. Typical TPD spectra for CO_2, N_2, and Ar at heating rates of about 17°C/min. Numbers denote peak temperatures in degrees centigrade.

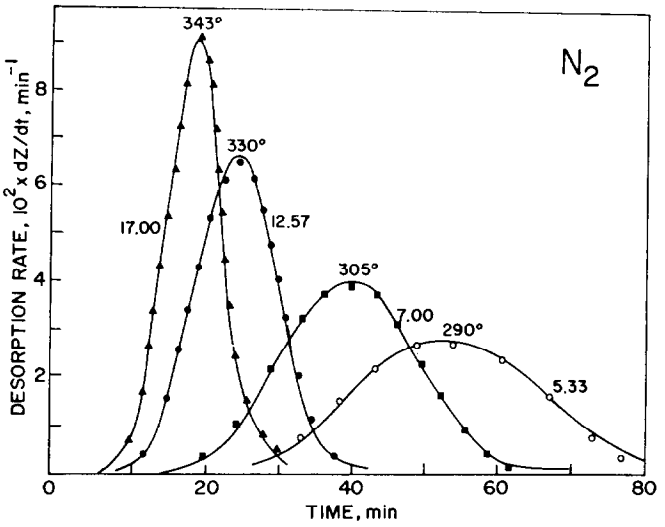

FIG. 6. TPD spectra for N_2 (solid curves) compared with calculated rates (points) for heating rates from 5.33 to 17.0°C/min. Numbers with degrees denote the temperatures of the peak maxima; other numbers, heating rates.

normal distribution was not used. The weight-average particle size was 3.5 μm, and the standard deviation, 1.49 μm. The present sample of 3A zeolite had smaller and more widely distributed particles than did the sample of 4A examined by Eagan and Anderson (*11*), which had a weight-average particle size of 4.0 μm and a standard deviation of 1.33 μm.

Figure 5 compares the TPD spectra of the three gases at heating rates of about 17°C/min. In these and subsequent figures, $dZ/dt = (1/Q_\infty)\, dQ/dt$, where dQ/dt is the rate of desorption at time t in cc (STP)/g per gram, and Q_∞ is the total amount desorbed in the experiment in the same units. CO_2 is more readily desorbed than is N_2 or Ar as shown by the relative posi-

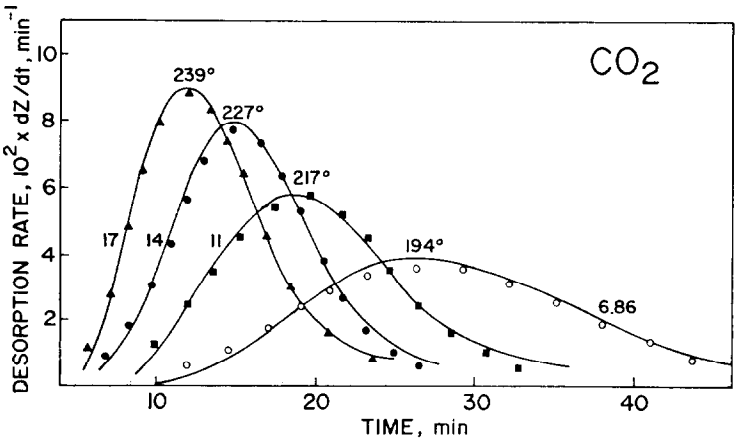

FIG. 7. TPD spectra for CO_2 (solid curves) compared with calculated rates (points) for heating rates from 6.86 to 17.0°C/min. Numbers with degrees denote the temperatures of the peak maxima; other numbers, heating rates.

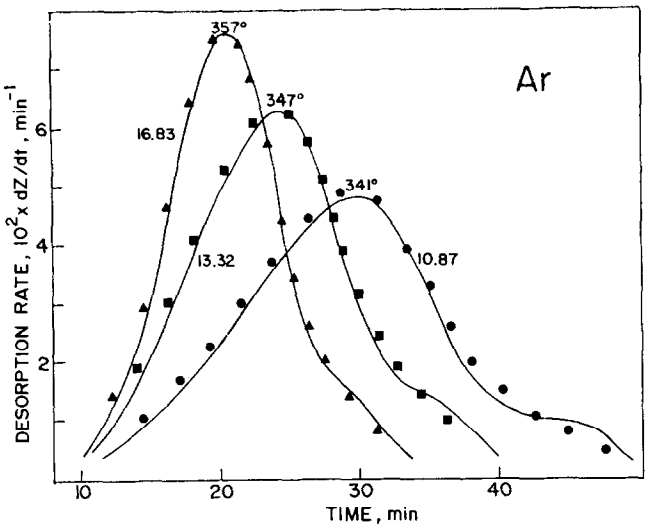

FIG. 8. TPD spectra for Ar (solid curves) compared with calculated rates (points) for heating rates from 10.87 to 16.83°C/min. Numbers with degrees denote the temperatures of the peak maxima; other numbers, heating rates.

tion of the curves and the temperatures of the peak maxima. The TPD curves for CO_2 and N_2 have a single peak, but Ar has two peaks. Figures 6–8 give TPD spectra for N_2, CO_2, and Ar, respectively, at different heating rates as continuous curves and rates calculated at particular times are shown as points. The calculations in Fig. 8 attempt to fit only the larger peak.

Figure 9 compares the TPD spectra for encapsulated argon with helium and with helium saturated with water vapor at room temperature, the water vapor being removed in a cold trap before reaching the

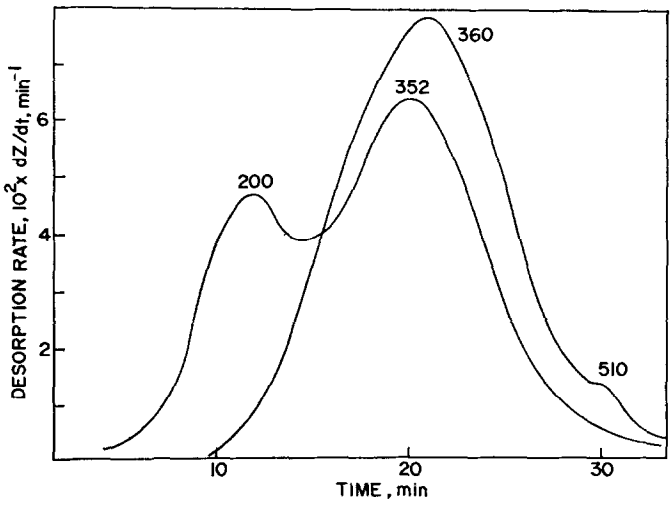

FIG. 9. TPD spectra for Ar using dry He as a carrier gas have peaks at 360 and 510°C. When the carrier gas was saturated with water vapor at 25°C, the peaks occurred at 200 and 352°C.

detector. In the presence of water vapor the large peak occurred at shorter times and lower temperatures, and the small peak disappeared.

DISCUSSION

Fick's second law of diffusion has often been used to interpret diffusion-controlled sorption data. Frequently, equations for diffusion of gas into or out of a porous solid are used without regard to adsorption and the shape of the adsorption isotherm. This approximation is used in the present work; however, at temperatures approaching the peak maxima, adsorption should be small and the adsorption isotherms should be nearly linear. Solutions of diffusion equations have been given by Crank (*12*). We will describe the solution for an infinite platelet and then transform this to the solution for cubes.

Consider a uniformly porous platelet of thickness $2a$ with a diffusivity D that is independent of concentration of diffusing species C, but is a function of temperature. The differential equation to be solved is

$$\partial C/\partial t = D(\partial^2 C/\partial x^2), \tag{1}$$

with the initial condition, $C = C_0$ at $t = 0$, at all positions within the platelet and the boundary conditions, $C = 0$ at $x = a$ and $x = -a$, and $dC/dx = 0$ at $x = 0$. By transforming variables with $X = x/a$ and $\tau = Dt/a^2$, Eq. (1) becomes

$$\partial C/\partial \tau = \partial^2 C/\partial X^2. \tag{2}$$

The fraction of the diffusing species that has left the platelet is finally obtained as

$$Z = 1 - (8/\pi^2) \times \sum_{n=0}^{\infty} \frac{\exp[-(2n+1)^2\pi^2\tau/4]}{(2n+1)^2}. \tag{3}$$

For long times, $\tau > 0.16$, and $Z > 0.45$, Eq. (3) reduces to

$$Z = 1 - (8/\pi^2)\exp(-\pi^2\tau/4), \tag{4}$$

and, for short times, $\tau < 0.16$, and $Z < 0.45$, another solution is available (*12*):

$$Z = 2(\tau/\pi)^{\frac{1}{2}}. \tag{5}$$

The equation for cubes can be obtained from the relationship (*11*), $(1 - Z_c) = (1 - Z_p)^3$, where the subscripts c and p denote cubes and platelets, as follows:

$$Z = 1 - (512/\pi^6) \times \sum_{0}^{\infty} \frac{\exp[-(2n+1)^2 3\pi^2\tau/4]}{(2n+1)^6}, \tag{6}$$

and, for long times, $\tau > 0.16$, and $Z > 0.83$,

$$Z = 1 - (512/\pi^6)\exp(-3\pi^2\tau/4), \tag{7}$$

and, for short times, $\tau < 0.16$, and $Z < 0.83$,

$$Z = 1 - [1 - 2(\tau/\pi)^{\frac{1}{2}}]^3. \tag{8}$$

For cubes, the parameter a is half of the edge length of the cube.

For the present experiments, which are not isothermal,

$$\tau = (1/a^2)\int_0^t D\,dt,$$

and $D = D_0\exp(-E/RT)$. For subsequent derivations, we note that

$$d\tau/dt = D/a^2 = (D_0/a^2)\exp(-E/RT).$$

By differentiating Eqs. (7) and (8) with respect to time, and expressing τ in terms of Z from these equations, and rearranging, linear Eqs. (9) and (10) are obtained.
For $Z < 0.83$:

$$\ln\left\{\frac{dZ}{dt}[1 - (1 - Z)^{\frac{1}{3}}](1 - Z)^{-\frac{1}{3}}(\pi/6)\right\} = \ln(D/\bar{a}^2) - E/RT. \tag{9}$$

For $Z > 0.83$:

$$\ln[(\tfrac{4}{3}\pi^2)(dZ/dt)/(1 - Z)] = \ln(D/\bar{a}^2) - E/RT, \tag{10}$$

where $\bar{a}$ is the weight mean half-cube-edge length. For Eqs. (9) and (10), plots of the

L. H. S. as a function of $1/T$ should give a straight line. These plots were linear from room temperature to about 100°C below the temperatures of the peak maxima. At higher temperatures the slope of the plot decreased and eventually became positive. Similar plots for simple first- and second-order desorption kinetics, frequently used in flash-desorption studies (*9*) and for the parabolic law, had the same pattern.

Equations (6)–(10) were obtained for a single particle size. The rate depends on D/a^2 and, thus, is strongly affected by a wide distribution of particle size. Hence, in the TPD experiments, very small particles desorb at a low temperature and soon become depleted of encapsulated gas; at higher temperatures desorption is mainly from larger particles, but at a relative lower rate because of the parameter D/a^2. Eagan and Anderson (*11*) and others (*13*) have demonstrated that the use of an average particle size is usually not adequate for explaining sorption kinetics properly.

A calculating scheme was devised that accounts for the distribution of particle sizes. Trial values of D_0 and E are introduced, and $\tau' = \int_0^t D dt$, where temperature T is related to t and heating rate β by $T = T_0 + \beta t$, is calculated for pertinent times. For each value of t the rate for each particle size is integrated over the particle size distribution to give a calculated rate that can be compared with the experimental rate. By a systematic procedure, the values of D_0 and E are adjusted to minimize the sum of squares of the difference of calculated and experimental rates.

The desorption rate for a single particle size, $dZ/dt = F(\tau', a)$, where a is the half-side length of the cube, can be calculated from the differential forms of Eqs. (5)–(7). The calculated overall rate is obtained by

$$\overline{dZ}/dt = \int_0^\infty P(a)F(\tau', a)da, \qquad (11)$$

where $P(a)$ is the probability distribution function in terms of weight, $P(a)\,da$ is the weight fraction of particles with sizes between a and $a + da$. The log-normal distribution function (*14*) is appropriate, as shown in Fig. 4, and is given as

$$P(a) = \{1/[(2\pi)^{\frac{1}{2}} a \ln \sigma]\} \times \exp - [(\ln a/\mu)/(2^{\frac{1}{2}} \ln \sigma)]^2,$$

where μ is the weight-average half-side length, and σ is the size below which 50 wt% of the particles lie divided by the size below which 15.87 wt% of the particles lie. With the transformation, $\omega = \ln (a/\mu)/2^{\frac{1}{2}} \ln \sigma$ and $d\omega = d \ln a/2^{\frac{1}{2}} \ln \sigma$, Eq. (11) becomes

$$\overline{dZ}/dt = \pi^{-\frac{1}{2}} \int_{-\infty}^{+\infty} \exp(-\omega^2) F(\tau', \omega) d\omega. \qquad (12)$$

This integration may be simplified by the relationship

$$\int_{-\infty}^{\infty} \exp(-\omega^2) f(\omega) d\omega = \sum_{i=1}^{m} H_i \cdot f(\omega_i),$$

where m is the order of the Hermite polynomial $H_m(\omega)$, ω_is are the roots of $H_m(\omega) = 0$, H_is are the weighting factors, and m was 8 in these calculations.

The integral,

$$\tau' = D_0 \int_0^t e^{-E/RT} dt,$$

was evaluated by the Romberg method (*15*). Initial calculations showed that the parameters D_0 and E were correlated; therefore, the parameters were changed to $D = D' \exp - [(E/R)(1/T - 1/T_c)]$, where $D' = D_0 \exp(E/RT_c)$, and T_c is an average temperature in degrees Kelvin. The values of D_0 and E obtained for the three gases are shown in Table 2, together with 95% confidence limits obtained from the least-square calculations. To test the Arrhenius parameters they were used to calculate diffusivities at 25°C, and these values are compared with diffusivities estimated from

TABLE 2

Diffusivity Coefficients ($D = D_0 \exp(-E/RT)$) of N_2, CO_2, and Ar in Zeolite 3A

Gas	$D_0 \times 10^5$ (cm²/s)	E (kcal/mol)	$D_{298°K} \times 10^{18}$ (cm²/s)
N_2	2.174 ± 0.138	17.34 ± 0.49	4.18 (10)[a]
CO_2	0.143 ± 0.021	13.04 ± 0.70	390.5 (65)[a]
Ar	0.303 ± 0.030	15.84 ± 0.82	7.32 (4)[a]

[a] Calculated from data of Fig. 2 using Eq. 8 and assuming uniform particle size.

data of Fig. 2 using Eq. (8), which assumes the particle size to be uniform and equal to the weight average. The data of Fig. 2 are scattered, each point being obtained in a separate experiment; therefore, the fact that the diffusivities at room temperature are of the same magnitude suggests that the parameters from the TPD tests are not grossly inaccurate.

Excellent agreement for calculated and experimental rates at four different heating rates was obtained for N_2 as shown in Fig. 6. For CO_2, fit was less exact, as shown in Fig. 7. For CO_2, the relatively large leakage rate depicted in Fig. 2 should develop concentration gradients within the particles before use. The theory is based on uniform concentration at the start of the experiment. In addition, CO_2 interacts more strongly with the zeolite and the diffusivity may be concentration dependent. For argon, the small second peak at about 500°C was ignored in the calculations shown in Fig. 8.

The two TPD peaks for argon suggest that the first maximum may be attributed to desorption from α cages, and the second, from β cages. Calculations were made for desorption from α and β cages assuming that 84% of the argon was contained in α cages and 16% in β cages, the relative volumes in the structure, and that gas desorbed from the β cages diffused freely through the α cages. These calculated results were not very much better than those in Fig. 8, and the second peak was not predicted properly. Apparently, the fraction of argon assigned to the β cages was too large.

When the carrier gas was saturated with water vapor at room temperature, the TPD spectra for argon were shifted to lower temperatures, and the second peak was not found (Fig. 9). Although interpretation of the spectra with water vapor is not simple, water would be expected to adsorb preferentially in the β cages. In other experiments with Ar in 3A, the temperature was held constant and water vapor was introduced intermittently for about 4-min periods. At 220°C the desorption rate was doubled by the presence of water vapor. The increase in rate on water addition decreased with increasing temperature and was about 15% at 360°C.

Nelson and Walker (*2*) and Walker *et al.* (*3*) reported the pre-exponential parameter for diffusivity in pelleted 3A zeolite in the form of $D_0^{\frac{1}{2}}/r$ obtained from equa-

TABLE 3

Comparison of Diffusivity Parameters

Gas	Present work		Literature		
	$D_0 \times 10^5$ (cm²/s)	E (kcal/mol)	D_0[a] (cm²/s)	E (kcal/mol)	Reference
N_2	2.174	17.3	0.764×10^{-5}	16.2	(*2*)
Ar	0.303	15.8	0.118×10^{-5}	14.0	(*2*)
			0.272×10^{-7}	12.5	(*3*)
CO_2	0.143	13.0	0.397×10^{-10}	4.0	(*3*)

[a] Calculated from literature data as described in text.

tions for spheres, but did not give crystallite size data. We have multiplied the $D_0^{\frac{1}{2}}/r$ values by the weight-average half-cube-edge-length, 1.75 μm, and squared the product to give the values of D_0 compared with those of the present work in Table 3. The agreement of the parameters for N_2 and Ar from Ref. (2) may be considered very good in view of the differences in initial amount of sorbed material, experimental methods, and the assumption made in changing the literature $D_0^{\frac{1}{2}}/r$ values to the form of the present data. Parameters obtained for CO_2 (*3*) are entirely different from ours, and the authors commented that these parameters were also inconsistent with their parameters obtained for N_2, Ar, Kr, and Xe (*3*).

Finally, we note that there seems to be no simple relationship between the diffusion parameters, E and D_0, and any of the estimates of molecular diameters and shape.

ACKNOWLEDGMENT

We express appreciation to the National Research Council of Canada for providing fellowship and operating funds, and to Dr. G. C. Gillies for assistance in the X-ray diffraction studies.

REFERENCES

1. Breck, D. W., *J. Chem. Educ.* **41**, 678 (1964).
2. Nelson, E. T., and Walker, P. L., Jr., *J. Appl. Chem.* **11**, 358 (1961); "Special Research Report SR-24." Department of Fuel Technology, Pennsylvania State University, University Park, Pa., 1961.
3. Walker, P. L., Jr., Austin, L. G., and Nandi, S. P., *Chem. Phys. Carbon*, **2**, 257 (1966); Walker, P. L., Jr., and Nandi, S. P., "Special Research Report SR-42." Department of Fuel Technology, Pennsylvania State University, University Park, Pa., 1964.
4. Barrer, R. M., and Vaughan, D. E. W., *Surface Sci.* **14**, 77 (1969).
5. Barrer, R. M., and Vaughan, D. E. W., *Trans. Faraday Soc.* **63**, 2275 (1967).
6. Barrer, R. M., and Vaughan, D. E. W., *J. Phys. Chem. Solids* **32**, 731 (1971).
7. Cvetanovic, R. J., and Amenomiya, Y., *Advan. Catal.* **17**, 103 (1967).
8. Smutzek, M., Cerny, S., and Buzek, F., *Advan. Catal.* **24**, 343 (1975).
9. Dawson, P. T., and Walker, P. C., *in* "Experimental Methods in Catalytic Research" (R. B. Anderson and P. T. Dawson, Eds.), Vol. 3, p. 211. Academic Press, New York, 1976.
10. Reed, T. B., and Breck, D. W., *J. Amer. Chem. Soc.* **78**, 5972 (1956).
11. Eagan, J. D., and Anderson, R. B., *J. Colloid Interface Sci.* **50**, 419 (1975).
12. Crank, J., "The Mathematics of Diffusion." Clarendon Press, Oxford, 1956.
13. Ruthven, D. M., and Loughlin, K. F., *Chem. Eng. Sci.* **26**, 577 (1971).
14. Irani, R. R., and Callis, C. F., "Particle Size Measurement, Interpretation, and Application." Wiley, New York, 1963.
15. McCalla, T. R., "Introduction to Numerical Methods and Fortran Programming." Wiley, New York, 1967.